

SIEVE TRAY EFFICIENCY USING CFD MODELING AND SIMULATION

Getye Gesit*

School of Chemical and Bio Engineering
Addis Ababa Institute of Technology, Addis Ababa University

ABSTRACT

In this work, computational fluid dynamics (CFD) models are developed and used to predict sieve tray hydrodynamics and mass transfer. The models consider the three-dimensional two-phase flow of vapor (or gas) and liquid in which each phase is treated as an interpenetrating continuum having separate transport equations. Interaction between the two phases occurs via interphase momentum and species mass transfers. For the CFD analysis, the commercial package CFX 14 of ANSYS was employed. Clear liquid height and vapor phase Murphree point and tray efficiencies are predicted for ten stages each of two distillation columns for two binary fluid systems. Predicted results are in agreement with selected existing correlations that have been accepted to give reasonably accurate predictions. The objective of the work was studying the extent to which CFD modeling and simulation can be used as a prediction and design tool and method for sieve tray mass transfer and efficiency. It is concluded that CFD modeling and simulation can be used as a powerful tool and method for sieve mass transfer modeling and simulation and hence can be used as a very valuable tool and method for tray design and analysis.

Keywords: Sieve Tray, Tray Efficiency, Tray Design and Analysis, CFD Modeling and Simulation, Mass Transfer

INTRODUCTION

Sieve trays are widely used as phase contacting devices. They are commonly used in distillation that is the dominant separation process of the chemical and related processing industries. They are also used in the closely related mass transfer operations of absorption and stripping as well as in liquid-liquid extraction. Low cost, high separation efficiency, simplicity of fabrication and non-proprietary nature are some of the reasons that make sieve trays the first choice and standard column internals. Sieve tray design information may also be extended to the design of other type of trays.

The mass transfer in sieve trays is affected by the prevailing hydrodynamics and heat transfer. The

hydrodynamics and mass and heat transfer give for each phase the time and spatial distribution fields of velocity, temperature, pressure, volume fraction, concentrations or compositions such as mole or mass fractions of species or components. From the concentration or composition distribution fields, efficiencies (point and tray efficiencies) can be calculated. These efficiencies are used not only to indicate the efficiency of mass transfer and separation but also are required in tray design to convert theoretical number of trays into actual number of trays.

An impasse that has hindered the further improvement of sieve trays is the fact that little is known about the flow phenomena prevailing inside a tray for given geometry and operating conditions. The main reason for this is the poor knowledge of the complex behaviours of the multiphase flow inside the tray. What hydrodynamics and heat and mass transfer to expect for given geometry and operating systems and conditions is not known, which is the major problem facing the current practice of tray design and analysis. As a result, current design and analysis of sieve trays are based on experience and empirical correlations. The spatial details of the multiphase flow field are lacking and the designer relies heavily on gross oversimplifications. These practices do not often take into account the actual hydrodynamics and heat and mass transfer processes inside the tray.

Therefore, better models and methods of modeling and predicting sieve tray hydrodynamics and heat and mass transfer are of paramount significance and in dire need. Once a method or methods are devised to solve the problem stated in the preceding paragraph, it will be possible to design trays having desired flow patterns that give rise to the best performance. Over the past years, only experimental methods could be thought of in solving such a problem. Although experimental methods are generally expected to give reliable data, the chaotic, three-dimensional and multiphase behaviours of the flow inside a tray severely limit the use of experimental methods and the amount of data they can give.

Recently, the development of powerful computers, advances in numerical methods, and improvements

* E-mail: getyegesit@gmail.com

in multiphase flow models permit the investigation of complex flow problems. The technique that combines these is computational fluid dynamics (CFD), a technique that is emerging as an important predictive and design tool for flows in process equipment. Compared to experimental methods, it gives complete information (time and spatial distributions of variables) and has relatively low cost and fast speed. A major advantage of CFD over experimental methods is its flexibility as it typically enables changing flow geometry and system conditions without incurring appreciable cost.

There have been few attempts made to model and predict sieve tray hydrodynamics using CFD [1,2]. In all of those works, the interphase drag relation of [2] was used. However, CFD simulations conducted here showed that the interphase drag relation of [2] fails to give correct results for high vapor density systems. There is one attempt made to model sieve tray mass transfer and predict efficiency using CFD [3]. As one limitation, the authors of [3] gave no relation for estimating bubble diameter. Also, what inlet composition values they used is not clear since these composition values are absent from the literature on which their work is based.

In this work, CFD models have been developed to model and simulate the hydrodynamics and mass transfer of a sieve tray and to predict tray and point efficiencies and clear liquid height. The prediction of the hydrodynamics and efficiencies of the sieve tray is given with a modeling of the downcomer region provided. Tray geometry and fluids are based on the works of Bennett et al. [4] and Yanagi and Sakata [5]. In the absence of experimental data, existing correlations were used for the CFD model validation and work comparison. Unlike that of Rahimi et al, [3], in the work here a relation is given for bubble diameter as can be seen from the model equations and the need for inlet composition values has been settled by making use of Aspen Plus modeling and simulation as indicated in the later sections of this paper.

The CFD simulation results are in agreement with the correlations of Bennett et al [4, 6]. The objective of the work was finding out the extent to which CFD modeling and simulation can be used as a design and prediction tool and method for species mass transfer and efficiency of sieve trays. From the results of this work, it can be concluded that CFD modeling and simulation can be used as an invaluable tool and method for tray design and analysis.

MODEL EQUATIONS

The model considers the flow of vapor (or gas) and liquid in the Eulerian-Eulerian framework in which each phase is treated as an interpenetrating continuum having separate transport equations. With the model focusing on the liquid-continuous region of the sieve tray as done in [4], the vapor phase is taken as the dispersed phase and the liquid phase as the continuous phase. Since the focus is on the species mass transfer behaviour of sieve trays, heat transfer has not been considered in this work. It should be noted that although the heat transfer affects the species mass transfer, the effect is small on a per tray basis. In addition, the modeling here is such that the heat transfer equation is uncoupled and there is no effect of heat transfer on the species mass transfer and there is no need to solve the heat transfer equation unless it is coupled and influential. Thus for each phase the time and volume averaged continuity, momentum and species mass transfer equations were numerically solved.

Continuity Equations Vapor phase

$$\frac{\partial}{\partial t}(r_G \rho_G) + \nabla \cdot (r_G \rho_G \mathbf{V}_G) = 0 \quad (1)$$

Liquid phase

$$\frac{\partial}{\partial t}(r_L \rho_L) + \nabla \cdot (r_L \rho_L \mathbf{V}_L) = 0 \quad (2)$$

Momentum Equations

Vapor phase

$$\begin{aligned} \frac{\partial}{\partial t}(r_G \rho_G) + \nabla \cdot (r_G \rho_G \mathbf{V}_G) = \\ -r_G \nabla p_G + \nabla \cdot (r_G \mu_{eff,G} (\nabla \mathbf{V}_G + (\nabla \mathbf{V}_G)^T)) \\ + r_G \rho_G \mathbf{g} - \mathbf{M}_{LG} \end{aligned} \quad (3)$$

Liquid phase

$$\begin{aligned} \frac{\partial}{\partial t}(r_L \rho_L) + \nabla \cdot (r_L \rho_L \mathbf{V}_L) = \\ -r_L \nabla p_L + \nabla \cdot (r_L \mu_{eff,L} (\nabla \mathbf{V}_L + (\nabla \mathbf{V}_L)^T)) \\ + r_L \rho_L \mathbf{g} + \mathbf{M}_{LG} \end{aligned} \quad (4)$$

Species Mass Transfer Equations

The transport equations for the mass fractions of the light component, LK, are:

Sieve Tray Efficiency using CFD Modeling and Simulation

Vapor phase

$$\begin{aligned} \frac{\partial}{\partial t}(r_G \rho_G Y_{LK}) + \nabla \cdot (r_G \rho_G \mathbf{V}_G Y_{LK}) \\ = \nabla \cdot (r_G \rho_G D_{LK,G} (\nabla Y_{LK})) \\ - S_{LG} \end{aligned} \quad (5)$$

Liquid phase

$$\begin{aligned} \frac{\partial}{\partial t}(r_L \rho_L X_{LK}) + \nabla \cdot (r_L \rho_L \mathbf{V}_L X_{LK}) \\ = \nabla \cdot (r_L \rho_L D_{LK,L} (\nabla X_{LK})) \\ + S_{LG} \end{aligned} \quad (6)$$

where Y_{LK} and X_{LK} are the mass fractions of the light component in the vapor phase and liquid phase, respectively.

Equations (1) to (6) are for the unsteady state case. For the steady state case, terms involving the time derivative are zero. As one source for the equations, the ANSYS CFX 14 Documentation [16] can be consulted.

The vapor (or gas) and liquid volume fractions, r_G and r_L , are related by the summation constraint.

$$r_G + r_L = 1 \quad (7)$$

The same pressure field has been assumed for both phases, i.e.,

$$p_G = p_L \quad (8)$$

$\mu_{eff,G}$ and $\mu_{eff,L}$ are the effective viscosities of the gas and liquid phases, respectively.

$$\mu_{eff,G} = \mu_{laminar,G} + \mu_{turbulent,G} \quad (9)$$

$$\mu_{eff,L} = \mu_{laminar,L} + \mu_{turbulent,L} \quad (10)$$

The term \mathbf{M}_{LG} in the momentum equations represents interphase momentum transfer between the two phases whereas S_{LG} is the interphase species mass transfer between the two phases.

Closure Relationships

In order to solve Eqs. (1) to (10) for velocities, pressure, volume fractions, and species mass fractions, we need additional equations that relate the interphase momentum transfer term \mathbf{M}_{LG} , the interphase species mass transfer term S_{LG} and the turbulent viscosities to the mean flow variables.

The interphase momentum transfer term \mathbf{M}_{LG} is basically interphase drag force per unit volume. With the gas as the dispersed phase, the equation for \mathbf{M}_{LG} is [16]

$$\mathbf{M}_{LG} = \frac{3}{4} \frac{C_D}{d_B} r_G \rho_L |\mathbf{V}_G - \mathbf{V}_L| (\mathbf{V}_G - \mathbf{V}_L) \quad (11)$$

For the low vapor density fluid system (cyclohexane n-heptane system 34 kPa), it was found from the CFD simulations that the interphase drag relation proposed by Van Baten et al, [2] better models the sieve tray hydrodynamics. For the relation proposed by Van Baten et al, the interphase momentum transfer term as a function of local variables and constant coefficients put in a form suitable for the CFD is:

$$\mathbf{M}_{LG} = \frac{(r_G^{average})^2}{(1 - r_G^{average}) V_S^2} g(\rho_L - \rho_G) r_G r_L |\mathbf{V}_G - \mathbf{V}_L| (\mathbf{V}_G - \mathbf{V}_L) \quad (12)$$

For the average gas holdup fraction, $r_G^{average}$, the correlation of Bennett et al. [6] was used:

$$r_G^{average} = 1 - \exp \left[-12.55 \left(V_S \sqrt{\frac{\rho_G}{\rho_L - \rho_G}} \right)^{0.91} \right] \quad (13)$$

For the high vapor density fluid system (isobutane n-butane system at 1138 kPa), it was found from the CFD simulations that the drag coefficient relation used in Rampure et al, [7] better models the sieve tray hydrodynamics. The relation is:

$$C_D = \left[\max \left\{ \frac{24}{Re} (1 + 0.15 Re^{0.687}), \frac{8}{3} \frac{E_O}{(E_O + 4)} \right\} \right] r_L^2 \quad (14)$$

where Re is the bubble Reynolds number and E_O is the Eotvos number.

The interphase species mass transfer term S_{LG} is basically the interphase mass transfer rate of the light component per unit volume. It is given by [16]:

$$S_{LG} = k_{LG}^c a_e (M_G \rho_{ML} Y_{LK} / K - \rho_L X_{LK}) \quad (15)$$

where

$$k_{LG}^c = \left(\frac{1}{k_L} + \rho_{ML} / (K \rho_{MV} k_G) \right)^{-1} \quad (16)$$

where a_e is the interfacial area per unit volume, M_G is the molecular weight of the gas/vapor, k_L and k_G

Getye Gesit

are the volumetric individual film mass transfer coefficients of the liquid and vapor, respectively, K is the mole fraction equilibrium ratio as in $y_e = Kx$, and ρ_{ML} and ρ_{MV} are the molar densities of the liquid and gas, respectively. K was taken from an equation of state thermodynamic method of the commercial process simulator Aspen Plus simulation of the distillation column of each fluid system.

Higbie's [8] relation has been widely used to predict mass transfer coefficients. Higbie's relations for the volumetric individual film mass transfer coefficients are:

$$k_L = 2 \sqrt{\frac{D_{LK,L}}{\pi \theta_L}} \quad (17)$$

$$k_G = 2 \sqrt{\frac{D_{LK,G}}{\pi \theta_G}} \quad (18)$$

where $D_{LK,L}$ and $D_{LK,G}$ are the diffusion coefficients of the light component in the liquid and vapor/gas, respectively. The contact times for liquid and vapor, θ_L and θ_G , respectively, in the liquid-continuous region are:

$$\theta_L = \frac{d_B}{V_{Rise}} = \frac{d_B^3 r_G^{average}}{V_S} \quad (19)$$

$$\theta_G = \frac{d_B}{V_H} \quad (20)$$

where d_B is the bubble diameter, $V_{Rise} = V_S/r_G^{average}$ is the rise velocity and V_H is the vapor velocity through the tray holes. V_S is the gas superficial velocity (velocity of vapor based on bubbling area of tray).

In the Introduction section, it was noted that one limitation of the work of Rahimi et al. [3] is that they give no relation for the bubble diameter d_B . In the present work here, d_B has been estimated using the relation for bubble diameter given in Bennett et al. [4]:

$$d_B = \left(\frac{-12/\sqrt{\pi} \frac{h_F \sqrt{V_H D_{LK,G}}}{V_{Rise} \ln(1-E_{OV})}}{1+m \frac{\rho_{MV}}{\rho_{ML}} \sqrt{\frac{V_H D_{LK,G}}{V_{Rise} D_{LK,L}}}} \right)^{2/3} \quad (21)$$

where the vapor phase point efficiency E_{OV} is estimated a priori from the Bennett et al. [4] correlation:

$$E_{OV} = 1 - \exp \left[\frac{-0.0029 \left(\frac{\rho_G V_H h_F}{\mu_G} \right)^{0.4136}}{1 + m \frac{\rho_{MV}}{\rho_{ML}} \sqrt{\frac{r_G^{average} D_{LK,G}}{D_{LK,L} \left(\frac{A_H}{A_B} \right)}} \left(\frac{h_L}{d_h} \right)^{0.6074} \left(\frac{A_H}{A_B} \right)^{-0.3195}} \right] \quad (22)$$

where the clear liquid height h_L was calculated using the Bennett et al. [6] correlation:

$$h_L = \alpha \left[h_w + C \left(\frac{Q_L}{\alpha L_w} \right)^{2/3} \right] \quad (23)$$

with $\alpha = 1 - r_G^{average}$ and $C = 0.501 + 0.439 \exp(-137.8 h_w)$. The froth height h_F was calculated from $h_F = h_L/\alpha$.

The interfacial area per unit volume a_e was calculated from

$$a_e = \frac{r_G}{d_B} \quad (24)$$

For the high pressure fluid system, k_L and k_G were multiplied by a factor of 0.9 so as to dump out over-predictions that were of the order of 6%.

For the liquid phase, the turbulence viscosities were related to the mean flow variables by using the standard k- ϵ turbulence model with default model coefficients. For the gas/vapor phase, the dispersed phase zero equation turbulence model was specified.

In the liquid phase light component mass transport equation, the eddy diffusivity of Bennett et al. [4] was used instead of the molecular diffusivity $D_{LK,L}$.

MODEL FLOW GEOMETRY

The model sieve tray geometry was selected based on the work of Yanagi and Sakata [5]. The model geometry and boundaries are shown in Fig. 1. The tray has a diameter of 1.213 m, a 0.925 m weir length, a weir height of 0.05 m, a downcomer clearance of 0.038 m, and a 10.2% hole area with 0.0127 m diameter holes. Solari et al. [9] and Solari

Sieve Tray Efficiency using CFD Modeling and Simulation

and Bell [10] assumed symmetric flow fields about the tray center. Making use of their assumptions, only half of the tray was modeled so as to save computational time and machine memory. The model includes the downcomer region. Liquid enters the tray through the downcomer clearance area, labelled Liquid Inlet, and leaves the flow geometry through the downcomer clearance area that leads to the tray below, labelled Liquid Outlet. Gas enters through holes at the bottom of the tray, labelled Vapor Inlet Holes, and leaves through holes at the top, labelled Vapor Outlet Holes.

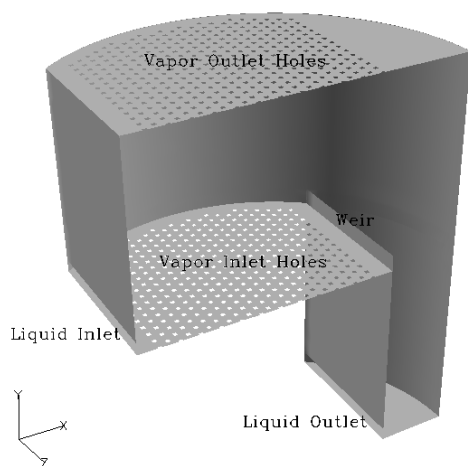


Figure 1 Model geometry and boundaries ($z = 0$ is the plane of symmetry, with the model geometry z coordinate values running from $z = 0$ down to $z = -0.6065$)

One of the geometry modeling problems faced was modeling the tray holes. Because of the relatively large tray diameter and high number of holes, working with the actual circular shape of holes proved to be computationally demanding because circular shapes are mesh or grid intensive. Hence square holes were used. This modeling approach was found to have insignificant effect on the tray hydrodynamics in a previous study [1].

The whole tray spacing (0.61 m) was considered in the simulation, even though the primary focus is in the froth region (about 0.20 m above the tray floor). This resulted in better numerical convergence, as well as provided with the ability to calculate tray efficiencies and clear liquid height.

OPERATING CONDITIONS AND SYSTEM PROPERTIES

Steady state CFD simulations were conducted for two binary fluid systems. The fluid systems and

operating conditions were based on the works of Bennett et al. [4] and Yanagi and Sakata [5] so that reasonable comparisons could be made. As two of their database fluid systems used in their correlation development, Bennett et al. [4] employed the two fluid systems of cyclohexane n-heptane and isobutane n-butane at 34 kPa and 1138 kPa, respectively. These were the fluid systems and operating pressures that Yanagi and Sakata [5] worked with. These two fluid systems and their operating pressures were used in this CFD work.

In order to assess the ability of the CFD models for modeling and simulating sieve tray hydrodynamics and interphase species mass transfer, CFD simulations were conducted for ten stages each of two distillation columns for the two binary fluid systems. Since the CFD simulations of mass transfer modeling and simulation need column stage profiles and properties, the RADFRAC module of the commercial process simulator Aspen Plus version 8 of AspenTech was used in rating mode to model and simulate each distillation column of each binary fluid system and generate column tray (or stage) profiles and properties. These profiles and properties were then used in the CFD work. The profiles and properties used from Aspen Plus simulations are given in Tables 1 and 2 in the Appendix.

The operating conditions and specifications used for the RADFRAC of Aspen Plus 8 were as follows. For the cyclohexane n-heptane system, used were: a feed rate of 8 mol/s at 20°C and 43 kPa containing 5 mol% cyclohexane, 31 stages including a total condenser and a kettle reboiler, feed stage \rightarrow 20, equilibrium stage model, distillate rate of 0.4 mol/s, mole fraction of cyclohexane in the distillate \rightarrow 0.99, top pressure \rightarrow 34 kPa, column pressure drop \rightarrow 12810 Pa, and thermodynamic method \rightarrow Peng-Robinson equation of state. For the isobutane n-butane system, used were: a feed rate of 0.001 mol/s with bubble point liquid at 1139.4 kPa containing 50 mol% isobutane, 12 stages including a total condenser and a kettle reboiler, feed stage \rightarrow 6, nonequilibrium stage model, distillate rate \rightarrow 5.0×10^{-4} mol/s, molar reflux ratio \rightarrow 1.6×10^5 so essentially total reflux condition, top pressure \rightarrow 1138 kPa, column pressure drop \rightarrow 2700 Pa, and thermodynamic method \rightarrow Peng-Robinson equation of state.

For both fluid systems, trays were numbered from top to bottom, the condenser being the 1st stage and the reboiler the last stage. CFD simulations were conducted for selected ten stages for each of the

two distillation columns. For the cyclohexane n-heptane system, selected were stages 2, 5, 8, 11, 14, 18, 21, 24, 27 and 30. For the isobutane n-butane system, selected were stages 2 to 11.

MODEL BOUNDARY CONDITIONS

To solve the continuity, momentum and species mass transfer equations, appropriate boundary conditions must be specified at all external boundaries plus at any specific internal boundaries of the flow geometry. For the hydrodynamics, boundary profiles were specified in line with a previous study [1]. For the species mass fractions, inlet values to stages calculated by the Aspen Plus simulations were used.

Liquid Inlet

For all simulations, uniform or flat inlet velocity profile was specified. The liquid volume fraction at the liquid inlet was taken to be unity assuming that only liquid enters through the downcomer clearance. The light component liquid phase mass fraction was specified to be the stage inlet mass fraction calculated using the Aspen Plus simulation. The vapor phase mass fraction of the light component was taken to be in equilibrium with the liquid phase.

Vapor Inlet

Uniform gas bubbling was used. The gas volume fraction at the inlet holes was specified to be unity. The light component vapor phase mass fraction was specified to be the stage inlet mass fraction calculated using the Aspen Plus simulation. The liquid phase light component mass fraction was taken to be in equilibrium with the vapor phase.

Liquid and Vapor Outlets

The liquid and vapor outlet boundaries were specified as outlet boundaries with normal speed specifications. At the liquid outlet, only liquid was assumed to leave the flow geometry and only gas was assumed to exit through the vapour outlet. These specifications will be in agreement with the specifications at the gas inlet and liquid inlet where only one fluid was assumed to enter.

Wall and Symmetry Boundaries

The no-slip wall boundary condition was used for both the gas and liquid phases. The symmetry plane was specified as a symmetry boundary.

SIMULATION RESULTS

The ability of the CFD simulations to predict and simulate sieve tray hydrodynamics and mass transfer behavior has been checked by calculating sieve tray clear liquid height and vapor phase Murphree point and tray efficiencies from the volume fraction and species mass fractions solution fields. Predicted vapor phase Murphree point and tray efficiencies are compared with the correlations of Bennett et al. [4] for ten stages each of two distillation columns for the two binary fluid systems. The computation and presentation of clear liquid height was done to show that the CFD models and simulations capture the appropriate sieve tray hydrodynamics. The sieve tray hydrodynamics influences the sieve tray mass transfer and efficiency. Computations of clear liquid height were made and the prediction results compared with values calculated from a correlation [6] that has been accepted to give accurate predictions.

The definitions and discussions of vapor phase Murphree point and tray efficiencies can be found in several standard textbooks on mass transfer operations and/or on distillation such as in [11-15]. The definition and method of calculation for clear liquid height can be found in a previous study [1].

The values of the point efficiency given in all figures are average values calculated from the averages of the four sieve tray edge values—two values from the edges near the inlet downcomer and two from the edges near the outlet weir. To picture where the edges are, the coordinates of the six vertices of the bubbling region of the model geometry are (0, 0, 0), (0, 0, -0.4625), (0, 0.61, 0), (0, 0.61, -0.4625), (0.7847, 0, 0), (0.7847, 0, -0.4625), (0.7847, 0.61, 0) and (0.7847, 0.61, -0.625). The four edges along which point efficiencies were computed are: (0, 0, 0) to (0, 0.61, 0), (0, 0, -0.4625) to (0, 0.61, -0.4625), (0.7847, 0, 0) to (0.7847, 0.61, 0), and (0.7847, 0, -0.4625) to (0.7847, 0.61, -0.4625). Distances are in meters.

Cyclohexane N-Heptane System at 34 kPa

Fig. 2 shows the CFD prediction of vapour phase Murphree tray efficiency compared with the values calculated using the correlation of Bennett et al. [4] for the system cyclohexane n-heptane at 34 kPa. The CFD predictions are in the right trend of and in general agreement with the correlation predictions (with an average relative absolute value error of 4.1%). The CFD predictions tended to slightly overpredict the Murphree tray efficiency. One

Sieve Tray Efficiency using CFD Modeling and Simulation

remedy tried during the simulations was multiplying the relations for k_L and k_G by a factor less than 1, say 0.85 or 0.9. That was found to damp out the over-predictions suggesting that the mass transfer coefficients input are optimistically higher. One possible source of discrepancy here and elsewhere is the fact that Bennett et al. [4] correlation considers only the liquid-continuous region. The vapor-continuous region also contributes to the tray efficiency and ignoring it may lower the correlation predicted efficiency. However, the results of this work for all the quantities here and elsewhere are quite acceptable given the large errors reported for other methods and relations in the literature [4].

Figure 3 gives the vapor phase Murphree point efficiency prediction of the CFD compared with the Bennett et al. [4] correlation prediction for the low pressure fluid system. The CFD predictions agree with the correlation predictions with an average relative absolute value error of 5.5%. The point efficiency as predicted by the CFD simulation varies from point to point inside the sieve tray whereas the Bennett et al. [4] correlation gives a single value for the tray. That could be one reason

for the discrepancy between the CFD predicted values and that of Bennett et al, [4] for the point efficiency. Another source of discrepancy is the ignoring of the vapor-continuous region in the correlation. As was observed for the tray efficiency, over-predictions possibly resulted from over-predictions of mass transfer coefficients.

In Fig. 4, the CFD prediction of clear liquid height is given compared against the Bennett et al. [6] correlation prediction for the low pressure fluid system. In this case, the CFD underpredicted the clear liquid height. It was observed that at high gas (or vapor) F-factor (as is the case for the low pressure fluid system), the CFD simulations tended to predict lower values of clear liquid height than the correlation of [6]. This means that the interphase drag relation used for the low pressure fluid system is predicting higher interphase drag than predicted for the correlation. The remedy is therefore to have a high gas F-factor dependent interphase drag relation or in general regime dependent interphase drag relation. However, such interphase drag relations are not (yet) available.

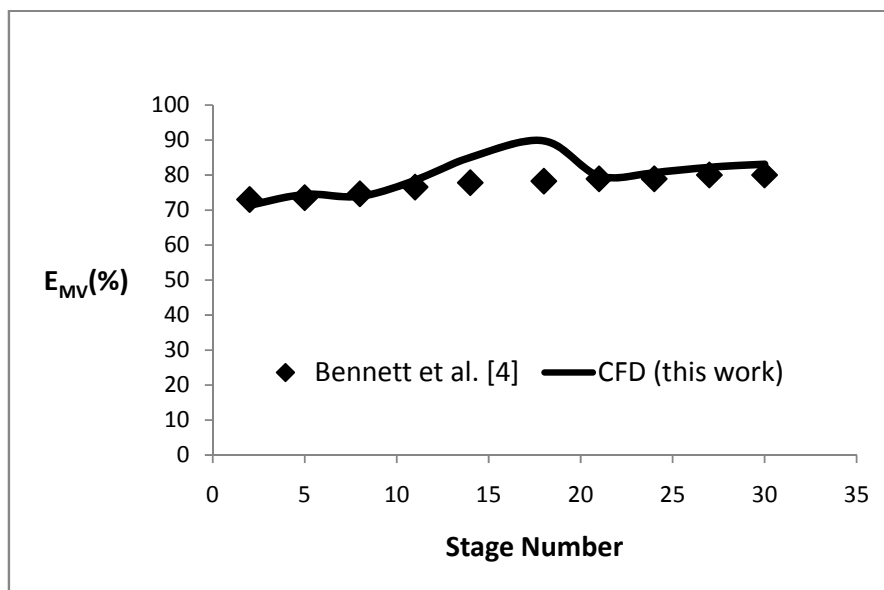


Figure 2 Vapor phase Murphree tray efficiency versus stage number for the cyclohexane n-heptane fluid system

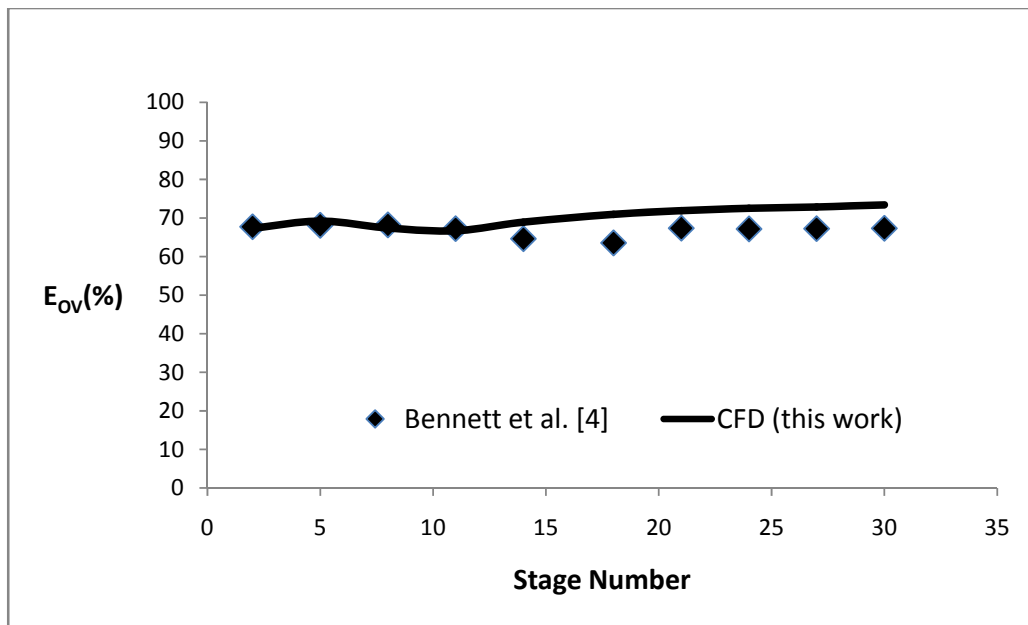


Figure 3 Vapor phase Murphree point efficiency versus stage number for the cyclohexane n-heptane fluid system

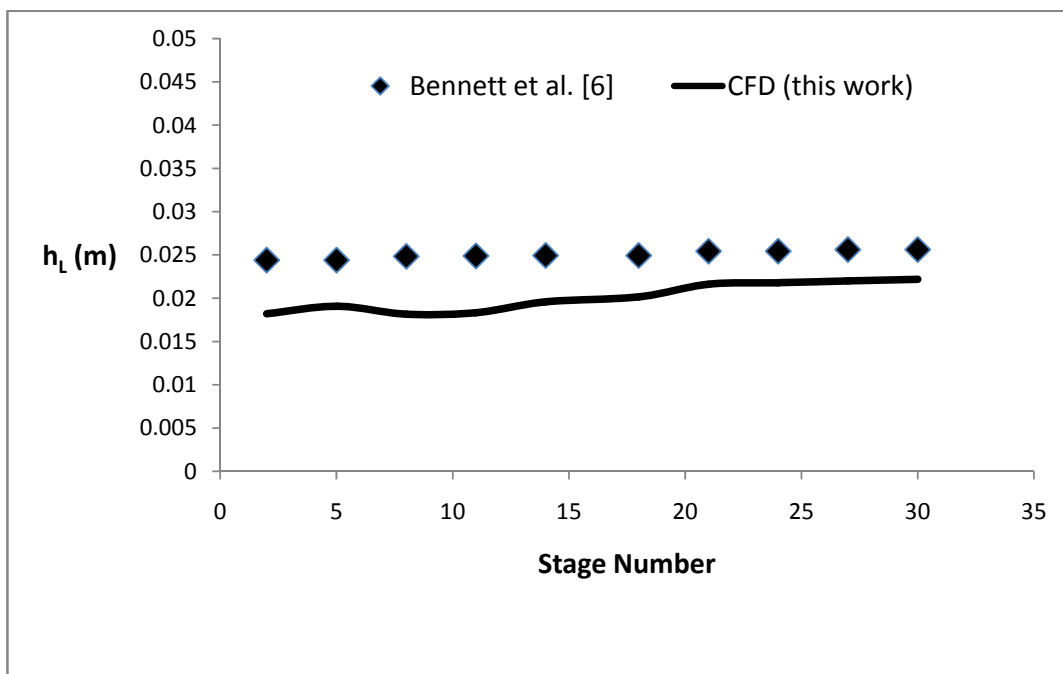


Figure 4 Clear liquid height versus stage number for the cyclohexane n-heptane fluid system

Sieve Tray Efficiency using CFD Modeling and Simulation

Isobutane N-Butane System at 1138 kPa

In Fig. 5, the CFD prediction of vapour phase Murphree tray efficiency is compared with the values calculated using the correlation of Bennett et al. [4] for the system isobutane n-butane at 1138 kPa. The CFD predictions are in good agreement with the predictions of the correlation of Bennette [4]. Fig. 6 gives the vapor phase Murphree point efficiency prediction of the CFD compared with the

Bennett et al. [4] correlation prediction for this high pressure fluid system. Here again, CFD predictions are in good agreement with the correlation predictions. In Fig. 7, the CFD prediction of clear liquid height is given compared against the Bennett et al. [6] correlation prediction for the high pressure fluid system. The CFD predicted clear liquid heights are in good agreement with the correlation predictions of [6].

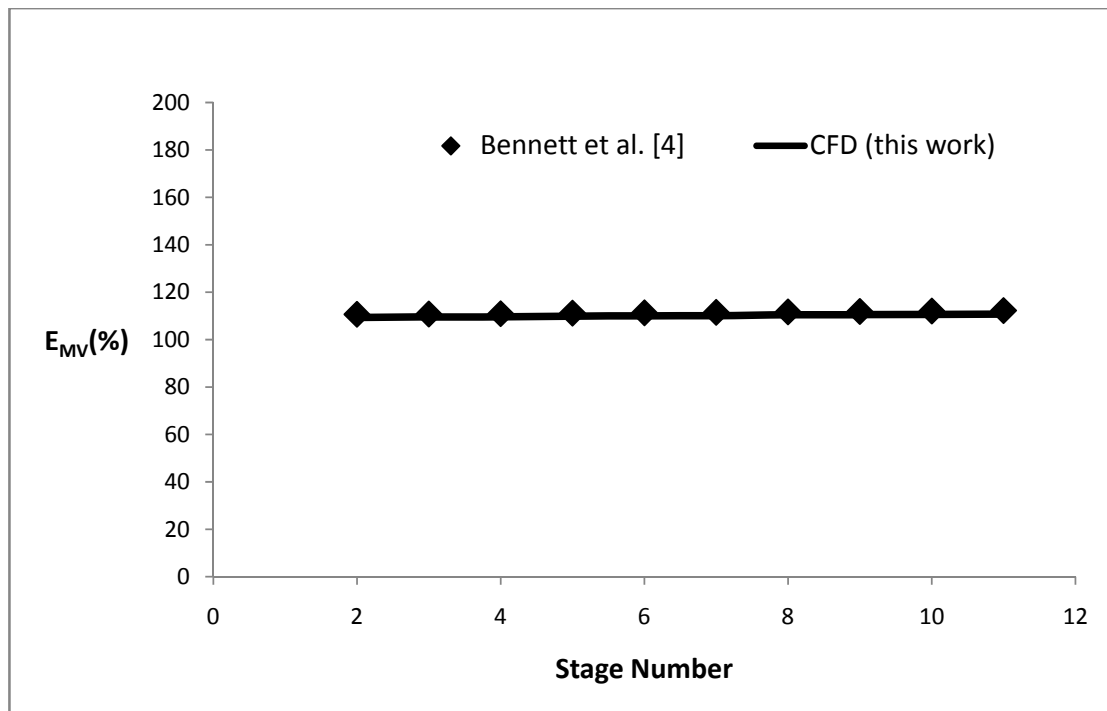


Figure 5 Vapor phase Murphree tray efficiency versus stage number for the isobutane n-butane fluid system

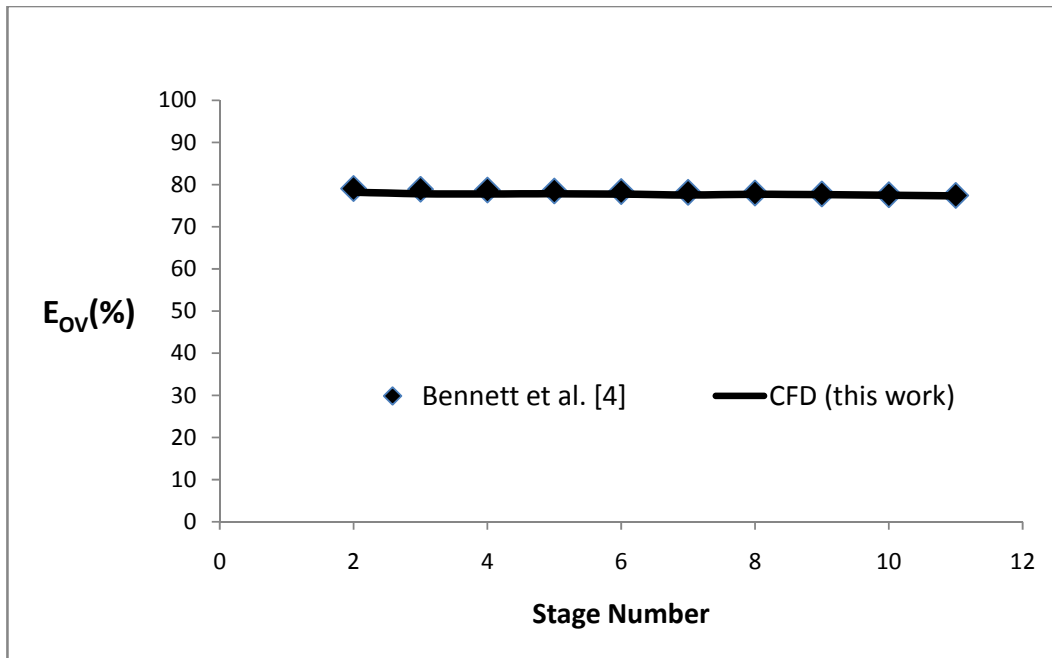


Figure 6 Vapor phase Murphree point efficiency versus stage number for the isobutane n-butane fluid system

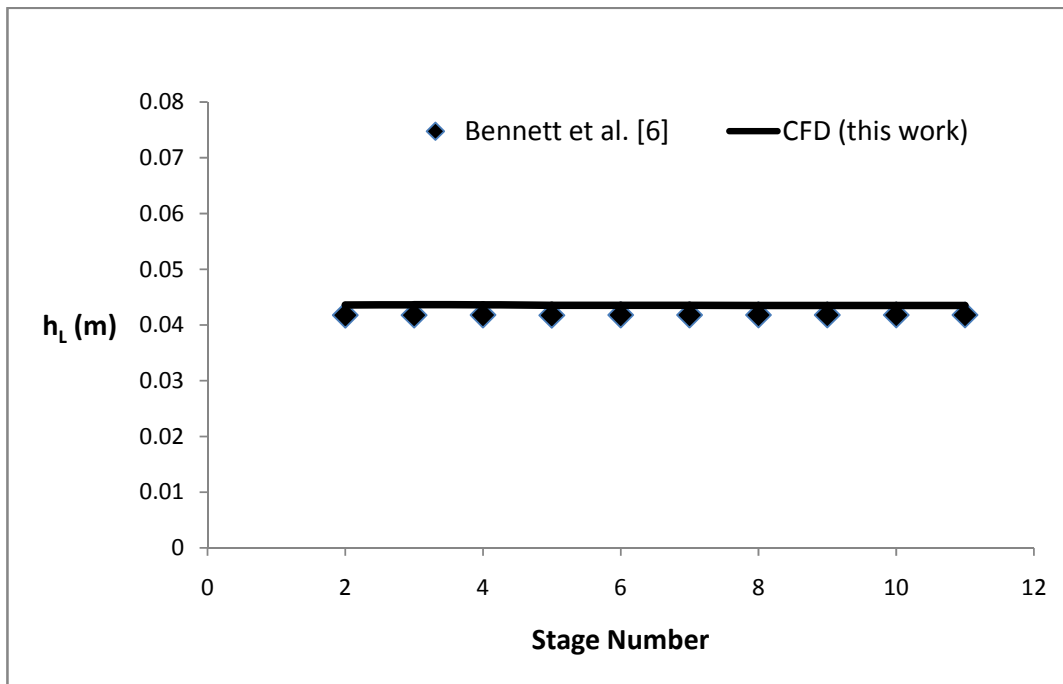


Figure 7 Clear liquid height versus stage number for the isobutane n-butane fluid System

Sieve Tray Efficiency using CFD Modeling and Simulation

Also, with geometry and operating conditions close to the work here, Yanagi and Sakata [5] experimentally found Murphree tray efficiency values close to the predictions here for the two fluid systems. Normal values of the experimental values are about 110% for the high pressure fluid system and about 75% for the low pressure fluid system. The high pressure fluid system exhibited higher efficiencies than the low pressure fluid system. This is so because of differences in the properties and conditions of the two fluid systems. For example, at the conditions and the properties used, the high pressure fluid system has smaller bubble diameter (about 7 mm for the high compared to about 14 mm for the low), relatively higher liquid phase mass diffusivity of the light component than the low pressure fluid system, and a higher clear liquid height (about 42 mm for the high compared to about 25 mm for the low). All of these give rise to increased species mass transfer and hence increased efficiency. The CFD modeling and simulation did not predict appreciable variation with stage of clear liquid height and efficiencies for both fluid systems. This is so because conditions and properties affecting the predicted quantities are close to one another on the different stages of the respective fluid system distillation column (see, for example, Table 1 in the Appendix).

One general indication that has been noted in the literature [11, 13] is that the Murphree tray efficiency can be greater than 100%. The CFD simulations here also indicate that the Murphree tray efficiency can be greater than 100% as is the case for the isobutane n-butane system. That of the low pressure system is less than 100%. It is also stated in the literature [11, 13] that the point efficiency is in the range of 0 to 100%. As has been indicated for the two fluid systems, the CFD prediction of point efficiency satisfies the constraint that point efficiency is in the range of 0 to 100%. Another observation that may be made is about the closure models for the two fluid systems considered in this study. Different closure relations were used for two fluid systems. This may mean that a single closure model cannot perhaps cover all fluid systems and operating conditions.

As is clear from the literature, satisfactory methods for calculating sieve tray efficiency are lacking. This work indicates that CFD modeling and simulation can be used as a powerful method for sieve tray efficiency calculation and for mass transfer modeling. The CFD modeling and simulation is by far superior compared to correlations used for sieve tray efficiency prediction which have many limitations. For

example, whereas the CFD gives the complete spatial distributions of the point efficiency, the correlations give unrealistically only a single value for the point efficiency.

CONCLUSION

This work provided validated models for modeling and predicting the hydrodynamics and mass transfer and predicting and calculating the efficiencies of sieve trays by means of computational fluid dynamics (CFD) using steady state simulations. The flow inside the tray was modeled as a three-dimensional two-phase flow of gas and liquid in the Eulerian-Eulerian framework. The time and volume averaged continuity, momentum and species mass transfer equations were numerically solved using the commercial package CFX 14 of ANSYS. The gas and liquid phase equations were coupled through appropriate interphase momentum and species mass transfer closure models. The CFD was used to predict clear liquid height and vapor phase Murphree point and tray efficiencies. The CFD simulation results are in good agreement with selected existing correlations predictions for the high pressure fluid system. For the low pressure fluid system, the CFD predictions agree to the correlation predictions of [4] with average relative absolute value errors of 4.1% for the Murphree tray efficiency and 5.5% for the point efficiency. The Murphree efficiency results are also close to experimentally found values [5] obtained using conditions and geometry close to this work.

Experiments for trays have proved to be difficult, expensive and time consuming. That is why only very few attempts have been made so far to determine sieve tray hydrodynamic and mass transfer behaviours. As a result, both data and methods for satisfactorily modeling and predicting sieve tray hydrodynamics and mass transfer and calculating efficiency are lacking. This work showed that CFD modeling and simulation can be used as a powerful tool and method for modeling and predicting sieve tray hydrodynamics and mass transfer and calculating tray efficiency. Modeling using CFD overcomes many of the limitations associated with experiments. Of paramount importance is its capability to give complete information (time and spatial distributions of variables) and the ease with which one can change tray geometry and operating conditions without incurring appreciable cost. It is concluded that CFD modeling and simulation can be used as a powerful tool and method for sieve tray mass transfer modeling and efficiency prediction and calculation

Getye Gesit

and hence can be used as a powerful tool and method for the design and analysis of sieve trays.

Nomenclature

A_B	tray bubbling area [m ²]
A_H	area of holes [m ²]
a_e	interfacial area per unit volume [m ² /m ³]
C_D	drag coefficient
$D_{LK,G}$	mass diffusivity of light component in the gas phase [m ² /s]
$D_{LK,L}$	mass diffusivity of light component in the liquid phase [m ² /s]
d_B	bubble diameter [m]
d_h	hole diameter [m]
E_{MV}	vapor phase Murphree tray efficiency
E_{OV}	vapor phase Murphree point efficiency
\mathbf{g}	gravitational acceleration vector [m s ⁻²]
g	gravitational acceleration [m s ⁻²]
h_F	froth height [m]
h_L	clear liquid height [m]
h_w	weir height [m]
k_G	volumetric individual film mass transfer coefficient in the gas phase [m/s]
k_L	volumetric individual film mass transfer coefficient in the liquid phase [m/s]
L_w	weir length [m]
m	slope of equilibrium curve
M_G	molar mass (molecular weight) of gas phase [kg/kmol]
\mathbf{M}_{LG}	interphase momentum transfer vector [kg m ⁻² s ⁻²]
p_G	gas phase pressure [N m ⁻²]
p_L	liquid phase pressure [N m ⁻²]
Q_L	liquid volumetric flow rate [m ³ /s]
r_G	gas (or vapor) phase volume fraction
$r_G^{average}$	average gas holdup fraction in froth
r_L	liquid phase volume fraction
S_{LG}	interphase species mass transfer [kg/(m ³ s)]
t	time [s]
\mathbf{V}_G	gas phase velocity vector [m/s]
V_H	hole velocity [m/s]
\mathbf{V}_L	liquid phase velocity vector [m/s]
V_S	gas phase superficial velocity based on bubbling area [m/s]
X_{LK}	mass fraction of light component in the liquid phase
x	mole fraction of light component in the liquid phase
Y_{LK}	mass fraction of light component in the vapor (or gas) phase
y_e	mole fraction of light component in the vapor phase in equilibrium with the liquid phase

Greek Letters

θ_G	contact time in the gas phase [s]
θ_L	contact time in the liquid phase [s]
$\mu_{eff,G}$	effective viscosity of gas [kg m ⁻¹ s ⁻¹]
$\mu_{eff,L}$	effective viscosity of liquid [kg m ⁻¹ s ⁻¹]
μ_G	molecular viscosity of gas [kg m ⁻¹ s ⁻¹]
ρ_G	gas phase mass density [kg/m ³]
ρ_L	liquid phase mass density [kg/m ³]
ρ_{MV}	gas phase molar density [kmol/m ³]
ρ_{ML}	liquid phase molar density [kmol/m ³]

REFERENCES

- [1] Gesit, G., Nandakumar, K. and Chuang, K. T., "CFD Modeling of Flow Patterns and Hydraulics of Commercial-Scale Sieve Trays", *AICHE Journal*, vol. 49, no. 4, 2003, pp. 910-924.
- [2] Van Baten, J. M. and Krishna, R., "Modelling Sieve Tray Hydraulics using Computational Fluid Dynamics", *Chemical Engineering Journal*, vol. 77, 2000, pp. 143-151.
- [3] Rahimi, R., Rahimi, M. R., Shahraki, F. and Zivdar, M., "Efficiencies of Sieve Tray Distillation Columns by CFD Simulation", *Chem. Eng. Technol.*, vol. 29, no. 3, 2006, pp. 326-335.
- [4] Bennett, D.L., Watson, D.N. and Wiescinski, M.A., "New Correlation for Sieve-Tray Point Efficiency, Entrainment, and Section Efficiency", *AICHE Journal*, vol. 43, no. 6, 1997, pp. 1611-1626.
- [5] Yanagi, T. and Sakata, M., "Performance of a Commercial Scale 14% Hole Area Sieve Tray", *Ind. Eng. Chem. Process Des. Dev.*, vol. 21, 1982, pp. 712-717.
- [6] Bennett, D. L., Agrawal, R. and Cook, P. J., "New Pressure Drop Correlation for Sieve Tray Distillation Columns", *AICHE Journal*, vol. 29, 1983, pp. 434-442.
- [7] Rampure, M. R., Kulkarni, A. A. and Ranade, V. V., "Hydrodynamics of Bubble Column Reactors at High Gas Velocity: Experiments and Computational Fluid Dynamics (CFD) Simulations", *Ind. Eng. Chem. Res.*, vol. 46, 2007, pp. 8431-8447.

Sieve Tray Efficiency using CFD Modeling and Simulation

- [8] Higbie, R., *Trans. AIChE*, vol. 31, 1935, pp. 365-389.
- [9] Solari, R. B., Saez, E., D'apollo, I. and Bellet, A., "*Velocity Distribution and Liquid Flow Patterns on Industrial Sieve Trays*", *Chem. Eng. Commun.*, vol. 13, 1982, pp. 369-384.
- [10] Solari, R. B. and Bell, R. L., "*Fluid Flow Patterns and Velocity Distribution on Commercial-Scale Sieve Trays*", *AIChE Journal*, vol.32, no. 4, 1986, pp. 640-649.
- [11] Treybal, R. E., "*Mass-Transfer Operations*", McGraw-Hill, 1980.
- [12] Kister, H. Z., "*Distillation Design*", McGraw-Hill, 1992.
- [13] Stichlmair, J. G. and Fair, J. R., "*Distillation: Principles and Practices*", Wiley-VCH, 1998.
- [14] Seader, J. D., Henley, E.J. and Roper, D.K., "*Separation Process Principles: Chemical and Biochemical Operations*", Wiley & Sons, 3rd Ed., 2011.
- [15] Lockett, M. J., "*Distillation Tray Fundamentals*", Cambridge University Press, Cambridge, 1986.
- [16] CFX 14 Help Documentation, ANSYS, Inc.

APPENDIX

Stage Profiles and Properties used from Aspen Plus Simulations

The stage profiles and properties used from Aspen Plus simulations are given in Tables 1 and 2 below. In both Tables, Q_L is liquid volumetric flow rate in m^3/s , Q_V is vapor volumetric flow rate in m^3/s , M_V is vapor molecular weight, M_L is liquid molecular

weight, ρ_L is liquid density in kg/m^3 , ρ_V is vapor density in kg/m^3 , μ_V is vapor dynamic viscosity in Ns/m^2 , σ is liquid surface tension in N/m , K_{LK} is equilibrium ratio of light component, K_{HK} is equilibrium ratio of heavy component, x is the mole fraction of the light component in the liquid, y is the mole fraction of the light component in the vapor, $D_{LK,L}$ is the molecular diffusivity of the light component in the liquid, and $D_{LK,V}$ is the molecular diffusivity of the light component in the vapor.

Table 1: Profiles and properties used from Aspen Plus simulations for the isobutane n-butane system

Stage	Q_L to	Q_V to	M_V to	M_L to	ρ_L to	ρ_V to	μ_V to
1	0.00E+00	1.59E-01	5.81E+01			2.93E+01	9.52E-06
2	9.57E-03	1.59E-01	5.81E+01	5.81E+01	4.86E+02	2.93E+01	9.53E-06
3	9.55E-03	1.58E-01	5.81E+01	5.81E+01	4.86E+02	2.92E+01	9.54E-06
4	9.53E-03	1.58E-01	5.81E+01	5.81E+01	4.86E+02	2.92E+01	9.55E-06
5	9.50E-03	1.58E-01	5.81E+01	5.81E+01	4.87E+02	2.92E+01	9.56E-06
6	9.48E-03	1.58E-01	5.81E+01	5.81E+01	4.87E+02	2.91E+01	9.57E-06
7	9.45E-03	1.58E-01	5.81E+01	5.81E+01	4.87E+02	2.91E+01	9.57E-06
8	9.43E-03	1.58E-01	5.81E+01	5.81E+01	4.87E+02	2.91E+01	9.58E-06
9	9.41E-03	1.58E-01	5.81E+01	5.81E+01	4.88E+02	2.90E+01	9.59E-06
10	9.39E-03	1.58E-01	5.81E+01	5.81E+01	4.88E+02	2.90E+01	9.60E-06
11	9.37E-03	1.57E-01	5.81E+01	5.81E+01	4.88E+02	2.90E+01	9.61E-06
12	9.35E-03	0.00E+00		5.81E+01	4.88E+02		

Table 1 (continued)

Stage	σ to	K_{LK}	K_{HK}	x	y	$D_{LK,L}$	$D_{LK,V}$
1		1.07E+00	8.65E-01	6.74E-01	7.18E-01	1.26E-08	
2	5.38E-03	1.07E+00	8.71E-01	6.46E-01	6.74E-01	1.26E-08	4.67E-07
3	5.37E-03	1.08E+00	8.76E-01	6.17E-01	6.46E-01	1.27E-08	4.68E-07
4	5.36E-03	1.09E+00	8.82E-01	5.87E-01	6.17E-01	1.28E-08	4.69E-07
5	5.36E-03	1.09E+00	8.87E-01	5.57E-01	5.87E-01	1.28E-08	4.70E-07
6	5.35E-03	1.10E+00	8.93E-01	5.26E-01	5.57E-01	1.29E-08	4.71E-07
7	5.34E-03	1.11E+00	8.99E-01	4.95E-01	5.26E-01	1.30E-08	4.72E-07
8	5.34E-03	1.11E+00	9.05E-01	4.64E-01	4.95E-01	1.30E-08	4.73E-07
9	5.33E-03	1.12E+00	9.11E-01	4.33E-01	4.64E-01	1.31E-08	4.74E-07
10	5.33E-03	1.13E+00	9.17E-01	4.03E-01	4.33E-01	1.32E-08	4.75E-07
11	5.32E-03	1.13E+00	9.22E-01	3.73E-01	4.03E-01	1.33E-08	4.76E-07
12	5.31E-03	1.14E+00	9.31E-01	3.26E-01	3.73E-01	1.34E-08	4.77E-07

Sieve Tray Efficiency using CFD Modeling and Simulation

Table 2: Profiles and properties used from Aspen Plus simulations for the cyclohexane n-heptane system

Stage	Q_L to	Q_V to	M_V to	M_L to	ρ_L to	ρ_V to	μ_V to
1	0.00E+00	1.43E+00	8.43E+01			1.10E+00	7.63E-06
2	2.06E-03	1.42E+00	8.44E+01	8.43E+01	7.48E+02	1.12E+00	7.63E-06
3	2.07E-03	1.40E+00	8.46E+01	8.44E+01	7.47E+02	1.13E+00	7.63E-06
4	2.08E-03	1.38E+00	8.48E+01	8.46E+01	7.45E+02	1.15E+00	7.62E-06
5	2.09E-03	1.37E+00	8.51E+01	8.48E+01	7.43E+02	1.16E+00	7.60E-06
6	2.10E-03	1.35E+00	8.57E+01	8.51E+01	7.39E+02	1.18E+00	7.57E-06
7	2.12E-03	1.33E+00	8.65E+01	8.57E+01	7.34E+02	1.20E+00	7.52E-06
8	2.15E-03	1.31E+00	8.77E+01	8.65E+01	7.26E+02	1.23E+00	7.45E-06
9	2.20E-03	1.29E+00	8.94E+01	8.78E+01	7.16E+02	1.26E+00	7.35E-06
10	2.26E-03	1.27E+00	9.16E+01	8.95E+01	7.03E+02	1.29E+00	7.22E-06
11	2.33E-03	1.24E+00	9.38E+01	9.17E+01	6.88E+02	1.33E+00	7.09E-06
12	2.41E-03	1.23E+00	9.58E+01	9.40E+01	6.74E+02	1.37E+00	6.98E-06
13	2.48E-03	1.22E+00	9.72E+01	9.61E+01	6.63E+02	1.39E+00	6.91E-06
14	2.53E-03	1.20E+00	9.82E+01	9.75E+01	6.55E+02	1.42E+00	6.86E-06
15	2.57E-03	1.19E+00	9.87E+01	9.85E+01	6.50E+02	1.44E+00	6.83E-06
16	2.60E-03	1.18E+00	9.91E+01	9.91E+01	6.48E+02	1.46E+00	6.82E-06
17	2.61E-03	1.17E+00	9.92E+01	9.94E+01	6.46E+02	1.47E+00	6.82E-06
18	2.62E-03	1.16E+00	9.93E+01	9.96E+01	6.45E+02	1.49E+00	6.82E-06
19	2.63E-03	1.15E+00	9.94E+01	9.97E+01	6.44E+02	1.50E+00	6.82E-06
20	3.79E-03	1.31E+00	9.96E+01	9.96E+01	6.58E+02	1.52E+00	6.82E-06
21	4.28E-03	1.30E+00	9.98E+01	9.98E+01	6.43E+02	1.54E+00	6.82E-06
22	4.30E-03	1.29E+00	9.99E+01	9.99E+01	6.42E+02	1.55E+00	6.82E-06
23	4.31E-03	1.28E+00	1.00E+02	1.00E+02	6.42E+02	1.57E+00	6.82E-06
24	4.32E-03	1.27E+00	1.00E+02	1.00E+02	6.41E+02	1.59E+00	6.82E-06
25	4.33E-03	1.26E+00	1.00E+02	1.00E+02	6.41E+02	1.60E+00	6.82E-06
26	4.34E-03	1.25E+00	1.00E+02	1.00E+02	6.40E+02	1.62E+00	6.83E-06
27	4.35E-03	1.24E+00	1.00E+02	1.00E+02	6.40E+02	1.63E+00	6.83E-06
28	4.35E-03	1.23E+00	1.00E+02	1.00E+02	6.39E+02	1.65E+00	6.84E-06
29	4.36E-03	1.22E+00	1.00E+02	1.00E+02	6.39E+02	1.66E+00	6.84E-06
30	4.37E-03	1.21E+00	1.00E+02	1.00E+02	6.39E+02	1.68E+00	6.85E-06
31	4.37E-03	0.00E+00		1.00E+02	6.38E+02		

Table 2 (continued)

Stage	σ to	K_{LK}	K_{HK}	x	y	$D_{LK,L}$	$D_{LK,V}$
1		1.00E+00	6.28E-01	9.90E-01	9.94E-01	4.42E-09	
2	2.02E-02	1.01E+00	6.29E-01	9.84E-01	9.90E-01	4.45E-09	8.61E-06
3	2.01E-02	1.01E+00	6.29E-01	9.75E-01	9.84E-01	4.47E-09	8.52E-06
4	2.00E-02	1.02E+00	6.29E-01	9.61E-01	9.75E-01	4.50E-09	8.44E-06
5	1.99E-02	1.02E+00	6.30E-01	9.38E-01	9.61E-01	4.53E-09	8.36E-06
6	1.97E-02	1.04E+00	6.31E-01	9.04E-01	9.40E-01	4.58E-09	8.29E-06
7	1.95E-02	1.06E+00	6.34E-01	8.52E-01	9.06E-01	4.63E-09	8.24E-06
8	1.93E-02	1.10E+00	6.42E-01	7.74E-01	8.55E-01	4.70E-09	8.21E-06
9	1.89E-02	1.17E+00	6.60E-01	6.64E-01	7.78E-01	4.81E-09	8.20E-06
10	1.83E-02	1.27E+00	6.96E-01	5.28E-01	6.72E-01	4.95E-09	8.22E-06
11	1.77E-02	1.40E+00	7.50E-01	3.84E-01	5.39E-01	5.12E-09	8.26E-06
12	1.70E-02	1.54E+00	8.12E-01	2.59E-01	3.98E-01	5.29E-09	8.31E-06
13	1.64E-02	1.66E+00	8.69E-01	1.66E-01	2.75E-01	5.44E-09	8.33E-06
14	1.60E-02	1.74E+00	9.12E-01	1.06E-01	1.85E-01	5.56E-09	8.33E-06
15	1.57E-02	1.80E+00	9.40E-01	7.04E-02	1.27E-01	5.64E-09	8.30E-06
16	1.55E-02	1.83E+00	9.56E-01	5.01E-02	9.15E-02	5.69E-09	8.26E-06
17	1.54E-02	1.85E+00	9.66E-01	3.88E-02	7.17E-02	5.73E-09	8.20E-06
18	1.53E-02	1.85E+00	9.71E-01	3.28E-02	6.07E-02	5.76E-09	8.14E-06
19	1.53E-02	1.86E+00	9.74E-01	2.95E-02	5.48E-02	5.79E-09	8.08E-06
20	1.67E-02	1.86E+00	9.76E-01	2.78E-02	5.16E-02	5.81E-09	8.01E-06
21	1.52E-02	1.87E+00	9.82E-01	2.04E-02	3.81E-02	5.85E-09	7.95E-06
22	1.51E-02	1.88E+00	9.87E-01	1.49E-02	2.79E-02	5.88E-09	7.89E-06
23	1.51E-02	1.88E+00	9.91E-01	1.08E-02	2.03E-02	5.91E-09	7.82E-06
24	1.50E-02	1.88E+00	9.93E-01	7.82E-03	1.47E-02	5.94E-09	7.75E-06
25	1.50E-02	1.88E+00	9.95E-01	5.62E-03	1.06E-02	5.97E-09	7.69E-06
26	1.49E-02	1.88E+00	9.97E-01	4.00E-03	7.54E-03	5.99E-09	7.63E-06
27	1.49E-02	1.88E+00	9.98E-01	2.82E-03	5.31E-03	6.02E-09	7.56E-06
28	1.49E-02	1.88E+00	9.98E-01	1.95E-03	3.68E-03	6.04E-09	7.50E-06
29	1.48E-02	1.88E+00	9.99E-01	1.32E-03	2.49E-03	6.06E-09	7.44E-06
30	1.48E-02	1.88E+00	9.99E-01	8.63E-04	1.62E-03	6.09E-09	7.38E-06
31	1.48E-02	1.88E+00	1.00E+00	5.26E-04	9.89E-04	6.11E-09	7.32E-06